THE JOURNAL OF BIOLOGICAL CHEMISTRY VOL. 286, NO. 19, pp. 17217–17226, May 13, 2011

Structure-dependent Impairment of Intracellular Apolipoprotein E4 Trafficking and Its Detrimental Effects Are Rescued by Small-molecule Structure Correctors*[S]

Received for publication, December 29, 2010, and in revised form, March 4, 2011 Published, JBC Papers in Press, March 18, 2011, DOI 10.1074/jbc.M110.217380

Jens Brodbeck[‡§], Jim McGuire[‡§], Zhaoping Liu[‡§], Anke Meyer-Franke[§], Maureen E. Balestra[‡§], Dah-eun Jeong[‡§], Mike Pleiss[§], Casey McComas[¶], Fred Hess[¶], David Witter[‖], Scott Peterson[‖], Matthew Childers[‖], Mark Goulet[‖], Nigel Liverton[¶], Richard Hargreaves[¶], Stephen Freedman[§], Karl H. Weisgraber[‡§‡‡§§], Robert W. Mahley[‡§**‡‡§§¶¶], and Yadong Huang[‡§**‡‡‖‖1]**

*From the [‡]Gladstone Institute of Neurological Disease, [§]Gladstone Center for Translational Research, **Gladstone Institute of Cardiovascular Disease, Departments of [¶¶]Medicine, [‡‡]Pathology, and [‖‖]Neurology, and the [§§]Cardiovascular Research Institute, University of California, San Francisco, California 94158, [¶]Merck Research Laboratories, West Point, Pennsylvania 19486, and [‖]Merck Research Laboratories, Boston, Massachusetts 02115*

Apolipoprotein (apo) E4 is the major genetic risk factor for Alzheimer disease (AD) and likely contributes to neuropathology through various pathways. Here we report that the intracellular trafficking of apoE4 is impaired in Neuro-2a cells and primary neurons, as shown by measuring fluorescence recovery after photobleaching. In Neuro-2a cells, more apoE4 than apoE3 molecules remained immobilized in the endoplasmic reticulum (ER) and the Golgi apparatus, and the lateral motility of apoE4 was significantly lower in the Golgi apparatus (but not in the ER) than that of apoE3. Likewise, the immobile fraction was larger, and the lateral motility was lower for apoE4 than apoE3 in mouse primary hippocampal neurons. ApoE4 with the R61T mutation, which abolishes apoE4 domain interaction, was less immobilized, and its lateral motility was comparable with that of apoE3. The trafficking impairment of apoE4 was also rescued by disrupting domain interaction with the small-molecule structure correctors GIND25 and PH002. PH002 also rescued apoE4-induced impairments of neurite outgrowth in Neuro-2a cells and dendritic spine development in primary neurons. ApoE4 did not affect trafficking of amyloid precursor protein, another AD-related protein, through the secretory pathway. Thus, domain interaction renders more newly synthesized apoE4 molecules immobile and slows their trafficking along the secretory pathway. Correcting the pathological structure of apoE4 by disrupting domain interaction is a potential therapeutic approach to treat or prevent AD related to apoE4.

The three isoforms of human apoE (apoE2, apoE3, and apoE4) differ at amino acid positions 112 or 158 or both (1, 2). ApoE4 is the major genetic risk factor for Alzheimer disease (AD)[2] (3–5), and apoE4 carriers account for 65–80% of all AD cases, highlighting the importance of apoE4 in AD pathogenesis (6). Two biophysical properties that distinguish apoE4 from the other isoforms likely hold the key to a mechanistic understanding of its association with AD. First, apoE4 is more unstable and tends to form a molten globule state (7, 8). Second, the amino-terminal domain (amino acids 1–191) of apoE4 interacts with its carboxyl-terminal domain (amino acids 223–299) (9, 10). This domain interaction occurs predominantly in apoE4, in which positively charged Arg-112 repels the side chain of Arg-61 in the amino-terminal domain, allowing the formation of a salt bridge between Arg-61 and the negatively charged Glu-255 in the carboxyl-terminal domain (9, 10). Domain interaction occurs to a significantly lesser extent in apoE2 and apoE3 because both have Cys-112, resulting in a different conformation of Arg-61 (11). Importantly, only human apoE has Arg-61; the 17 other species in which the apoE gene has been sequenced have Thr-61 (2, 11). Mutation of Arg-61 to Thr in apoE4 prevents domain interaction, converting apoE4 to an apoE3-like molecule (9–12). ApoE4 domain interaction occurs on lipoprotein particles *in vitro* in human plasma, in cultured Neuro-2a cells, and in Arg-61 knock-in mice, in which domain interaction was introduced into mouse apoE by mutating Thr-61 to Arg (9, 10, 12, 13). It has been suggested that domain interaction is a molecular basis for some of the apoE4 detrimental effects in neurobiology, as preventing or disrupting domain interaction corrects those effects (11, 14–16).

The central nervous system contains high levels of apoE mRNA, second in abundance only to the liver (17). ApoE is the major apolipoprotein in cerebrospinal fluid and is derived from the brain, not the periphery (18). Initially, it was thought that apoE in the central nervous system is exclusively synthesized by astrocytes, oligodendrocytes, activated microglia, and ependymal layer cells (19, 20). We now know that under diverse pathophysiological conditions, central nervous system neurons also

* This work was supported by Merck Research Laboratories. This work was also supported, in part, by National Institutes of Health Grant P01 AG022074.

[S] The on-line version of this article (available at http://www.jbc.org) contains a supplemental movie.

[1] To whom correspondence should be addressed: 1650 Owens St., San Francisco, CA 94158. Tel.: 415-734-2511; Fax: 415-355-0824; E-mail: yhuang@gladstone.ucsf.edu.

[2] The abbreviations used are: AD, Alzheimer disease; ER, endoplasmic reticulum; FRAP, fluorescence recovery after photobleaching; EGFP, enhanced green fluorescent protein; RFP, red fluorescent protein; APP, amyloid precursor protein; DIV, days *in vitro*.

express apoE (21–26). Neuronal production of apoE4 in response to stress or injury may be important in mediating its detrimental effects in AD pathogenesis (14–16).

ApoE is a secreted protein, and its production and transit through the secretory pathway in neurons could be affected by many factors, including its folding status, as demonstrated for other secreted proteins (27–31). We hypothesized that the biophysical characteristics of apoE4, notably domain interaction, affect its folding and, thus, its trafficking from the endoplasmic reticulum (ER) through the Golgi apparatus to the cell membrane. To test this hypothesis, we transfected Neuro-2a cells and mouse primary hippocampal neurons with cDNA constructs encoding enhanced green fluorescent protein (EGFP)-tagged apoE proteins (apoE3, apoE4, and apoE4-R61T) as a noninvasive probe to measure fluorescence recovery after photobleaching (FRAP), a powerful technology that can monitor intracellular trafficking of cargo proteins (32). Here we report that apoE3 and apoE4 have different intracellular trafficking profiles in neuronal cells, as domain interaction causes more apoE4 than apoE3 molecules to be retained in the ER and Golgi and to move more slowly along the secretory pathway.

EXPERIMENTAL PROCEDURES

Expression Constructs—cDNAs of apoE3 and apoE4 were subcloned into pcDNA3 expression vectors in-frame with the amino-terminal apoE signal sequence followed by EGFP and apoE with a stop codon to generate EGFP-apoE3 and EGFP-apoE4. EGFP-apoE4-R61T was prepared by site-directed mutagenesis of EGFP-apoE4 (QuikChange, Stratagene, La Jolla, CA). EGFP-apoE3, EGFP-apoE4, and EGFP-apoE4-R61T were also subcloned into a Sindbis viral vector for transduction of mouse primary hippocampal neurons. Red fluorescent protein (RFP) ER marker (RFP-ER) was from Invitrogen. An amyloid precursor protein (APP)-EGFP construct was a gift from Lennart Mucke (Gladstone Institute of Neurological Disease).

Neuro-2a Cell Culture—Wild type Neuro-2a neuroblastoma cells (CCL-131 ATCC, Manassas, VA) were cultured in minimum essential medium supplemented with 10% fetal bovine serum (Invitrogen), 1% sodium pyruvate (100 mM, Invitrogen), and 1% L-glutamine (200 mM, Invitrogen) in 75-cm^2 flasks at 37 °C in 5% CO_2 in a humidified incubator. Cells were subcultured twice weekly (dilution 1:4) and dislodged from the flask with trypsin solution. Neuro-2a cells stably expressing human apoE3 or apoE4 at similar levels were generated in our laboratory (24, 26).

Generation of Neuro-2a Cells Stably Expressing Different Forms of EGFP-apoE—Neuro-2a cells were transfected with EGFP-apoE3, EGFP-apoE4, and EGFP-apoE4-R61T using Lipofectamine 2000 (Invitrogen) and selected with 400 μg/ml neomycin (Invitrogen) for 4 weeks. Colonies with green fluorescence were picked for further enrichment.

Mouse Primary Hippocampal Neuron Culture and Transient Expression of ApoE—Primary hippocampal neuronal cultures were prepared on postnatal day 0 pups of apoE knock-out mice as reported (33). Hippocampi were isolated, and dissociated cells were plated in 8-well chamber slides with a coverglass bottom (Nunc, Roskilde, Denmark) coated with PL-lysine (Sigma) at 20,000 cells/well in Neurobasal medium supplemented with B27, 100 units/ml penicillin G, and 100 μg/ml streptomycin. At 13 days *in vitro* (DIV) culture, primary neurons were transduced with Sindbis virus expressing EGFP-apoE3, EGFP-apoE4, or EGFP-apoE4-R61T. At 14 DIV, the intracellular trafficking of different forms of EGFP-apoE was analyzed.

Small-molecule Structure Correctors—Two small-molecule structure correctors were used in the current study. One, GIND25, disrupts apoE4 domain interaction (Ye *et al.* (36)). The other is a newly identified phthalazinone derivative, 4-{4-[2-(3-methyl-4-oxo-3,4-dihydro-phthalazin-1-yl)-acetyl-amino]-benzyl}-piperazine-1-carboxylic acid *tert*-butyl ester (PH002, Merck) that disrupts apoE4 domain interaction more potently than GIND25.

Confocal Microscopy—For FRAP measurements, cells were plated 2 days before the experiment in eight-well chamber slides with a coverglass bottom (Nunc) coated with PL-lysine (Sigma) at 5000 cells/well. Recordings were obtained with an inverted Leica SP5 confocal microscope (Leica Microsystems, Wetzlar, Germany) and a 63× oil objective with a numerical aperture of 1.4; cells were maintained at 37 °C in 5% CO_2. Recording parameters were chosen to minimize light exposure to 1 milliwatt outside of the 20-milliwatt high-intensity laser bleaches with an argon laser at 488 nm for 1.2 s. A stable base line ensured that the EGFP fluorophore was not photo-damaged during pre-bleach base line and post-bleach recovery plateau recordings. Morphologic identification of the ER and Golgi apparatus was confirmed by cotransfection of RFP-ER in Neuro-2a cells.

Image Analysis of FRAP—Fluorescence intensity values were exported into Excel. Fluorescence levels were normalized to their pre-bleach base lines, and the extent of recovery was determined (32). The mobile fraction (%) was defined as the post-bleach recovery plateau; the immobile fraction (%) was calculated as the pre-bleach base line minus the post-bleach recovery plateau. To determine half-maximal recovery times, post-bleach fluorescence values were normalized to the values of the post-bleach recovery plateau, and the time of the 50% recovery value was determined.

Diffusion Coefficient D—The diffusion coefficient D was calculated for a circular beam, assuming Gaussian diffusion from the equation $D = (w^2/4\tau_{½})\ \gamma_D$, where w is the radius of the laser beam, $\tau_{½}$ is the time required for the bleached spot to recover half of its initial integrated intensity, and γ_D is the bleach factor (32).

Neurite Outgrowth Assay—Neuro-2a cells stably expressing apoE3 or apoE4 were seeded at 7500–8000 cells/well on PL-lysine-coated 24-well plates containing Opti-MEM with either 0.03% DMSO (control) or DMSO plus compound PH002 (100 nM). Cells were grown for 72 h at 37 °C to induce neurite outgrowth. After fixation with 4% paraformaldehyde for 30 min, cells were washed with PBS, stained with a SimplyBlue Safe Stain kit (Invitrogen) for 2 h, and washed again with PBS. Bright-field images were obtained with a Zeiss Axio Observer Z1 microscope (equipped with a motorized stage) and Volocity software. For each well, eight images were automatically taken from the same fields. Images were analyzed with NIH Image J to

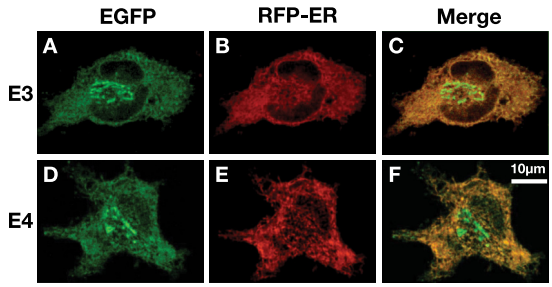

FIGURE 1. **EGFP-apoE3 and EGFP-apoE4 localize to the ER and Golgi apparatus in Neuro-2a cells transiently transfected with RFP-ER.** *A–F*, representative confocal images of EGFP-apoE (*green*) and RFP-ER (*red*) fluorescence in Neuro-2a cells expressing EGFP-apoE3 (*A–C*) or EGFP-apoE4 (*D–F*) are shown. The distinct morphology of the perinuclear Golgi apparatus with the strongest EGFP-apoE fluorescence is apparent.

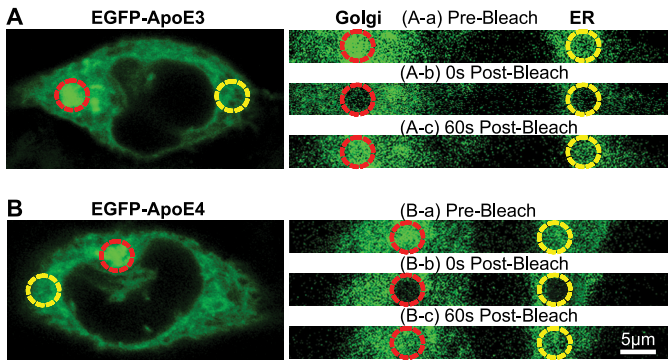

FIGURE 2. **FRAP measurements in Neuro-2a cells stably expressing different forms of EGFP-apoE.** *A* and *B*, representative confocal images of EGFP-apoE3 (*A*) and EGFP-apoE4 (*B*) fluorescence in Neuro-2a cells are shown. Areas exposed to the laser beam are indicated by *red* (Golgi apparatus) and *yellow* (ER) circles. *A* and *B*, *a–c*, shown are the respective area before bleaching (*a*), 0 s after bleaching (*b*), and after a 60-s recovery period (*c*).

determine the total cell count per image and to identify cells with neurites longer than the cell body diameter.

Dendritic Spine Quantification—Hippocampal primary neurons were cultured from P0 pups of NSE-apoE3 and NSE-apoE4 transgenic mice (33). At 5 DIV, primary neurons were transiently transfected with EGFP-β-actin to highlight dendritic spines (34). At 11 DIV, some of the primary neurons expressing apoE3 or apoE4 were treated with PH002 (100 nM for 3 days). At 14 DIV, all cells were fixed with ice-cold 4% paraformaldehyde in PBS (pH 7.4) and mounted on microscope slides with Vectashield (Vector Laboratories). Digital images of EGFP were collected on a laser-scanning confocal microscope with a Bio-Rad Radiance 2000 scanhead mounted on an Optiphot-2 microscope (Nikon) with a 60× oil objective lens. The dendritic spine densities were quantified as described (34).

Statistical Analyses—Values are expressed as the mean ± S.D. Statistical analyses were performed with GraphPad Prism. Differences between means were assessed by *t* test, Mann-Whitney *U* test, or one-factor analysis of variance. $p < 0.05$ was considered statistically significant.

RESULTS

EGFP-apoE Localizes to the ER and Golgi Apparatus in Neuro-2a Cells—Neuro-2a cells stably expressing EGFP-tagged apoE3 or apoE4 were established by transfection of cDNAs encoding the respective fusion protein starting with the signal peptide of apoE. Stably transfected cells were selected for neomycin resistance. Expression of the EGFP-apoE fusion proteins was confirmed visually by their green fluorescence and biochemically by SDS-PAGE and Western blotting with polyclonal anti-apoE, giving rise to a band of the expected size of ~65 kDa with comparable intensity for both expressed apoE isoforms. Examination of the cell lines by confocal microscopy revealed EGFP-apoE throughout the cell in a reticulate structure that co-localized with RFP-ER (Fig. 1). Concentrations of the fusion proteins were highest in the perinuclear region with the characteristic morphology of the Golgi apparatus, which was negative for RFP-ER (Fig. 1). No obvious distribution differences were apparent between the expressed EGFP-apoE3 and EGFP-apoE4 (Fig. 1). Thus, the EGFP-tagged apoE isoforms have a normal intracellular distribution pattern in Neuro-2a cells, as reported for wild type apoE3 and apoE4 (13, 35).

Greater Retention of ApoE4 Than ApoE3 in the ER and Golgi Apparatus of Neuro-2a Cells—To assess isoform-specific differences in apoE trafficking within the secretory pathway, we conducted FRAP measurements in Neuro-2a cells stably expressing EGFP-apoE3 or EGFP-apoE4 (Fig. 2). Base-line fluorescence was recorded for 10 s at 12.5 frames/s and low- intensity illumination (1 milliwatt) (Fig. 2, *Aa* and *Ba*). A 20-milliwatt high-energy circular argon laser beam (diameter, 5 μm; wavelength, 488 nm) was focused for ~1.2 s on the ER or Golgi apparatus of individual Neuro-2a cells (Fig. 2, *Ab* and *Bb*). In both compartments, the fluorescence of EGFP molecules was reduced to ~40% of base-line levels. The extent of bleaching was similar for both apoE isoforms (Fig. 3, *A* and *B*). During continuous recording at low-intensity illumination (1 milliwatt) after bleaching, unbleached molecules outside the bleached area, driven by active transport or diffusion, replaced mobile bleached molecules within the bleached area. This recovery of fluorescence intensity reached a plateau within 60 s (Fig. 2, *Ac* and 2*Bc* and Fig. 3, *A* and *B*).

The extent of the fluorescence recovery (*i.e.* the mobile fraction) in the ER and Golgi apparatus was significantly lower in EGFP-apoE4-expressing cells than in EGFP-apoE3-expressing cells, reaching 73.3 ± 3.7 and 71.7 ± 4.4% and reaching 86.1 ± 5.7 and 85.7 ± 2.8% of base-line fluorescence, respectively (Fig. 3, *A* and *B*). The fluorescence intensity of the recovery plateau was lower than the pre-bleach base line, as some molecules were retained in the bleached area and are, therefore, not replaced by unbleached molecules during the experiment. Thus, the difference in fluorescence intensity between the pre-bleach base line and the recovery plateau-level reflects the immobile fraction (32). The immobile fraction of apoE4 was about 100% higher than that of apoE3 in both the ER (26.7 ± 3.7% *versus* 13.9 ± 5.7%) and Golgi apparatus (28.3 ± 4.4% *versus* 14.3 ± 2.8%) (Fig. 3*C*).

ApoE4 Trafficking Is Slower Than ApoE3 in the Golgi Apparatus of Neuro-2a Cells—To measure the mobility of EGFP-apoE molecules along the secretory pathway, we determined the half-maximal fluorescence recovery times in the ER and Golgi apparatus (Fig. 3, *D* and *E*). In the Golgi apparatus, EGFP-apoE4 molecules reached half-maximal recovery more slowly than EGFP-apoE3 molecules (8.9 ± 2 *versus* 4.7 ± 1.1 s); how-

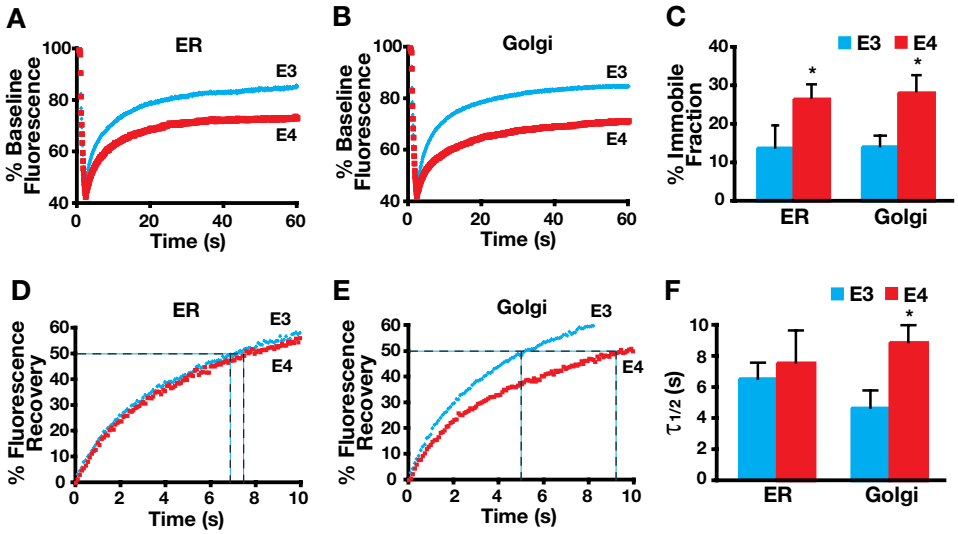

FIGURE 3. **ApoE4 decreases fluorescence recovery in the ER and Golgi apparatus and slows fluorescence recovery in the Golgi apparatus of Neuro-2a cells.** *A* and *B*, FRAP measurements of EGFP-apoE3 and EGFP-apoE4 in the ER (*A*) and Golgi apparatus (*B*) are shown. The fluorescence recovery plateau of EGFP-apoE4 in the ER and Golgi apparatus is 14% lower than that of EGFP-apoE3. *C*, in the ER and Golgi apparatus, the immobile fraction of EGFP-apoE4 is ~100% higher than that of EGFP-apoE3. *D* and *E*, shown are fluorescence recovery kinetics of EGFP-apoE3 and EGFP-apoE4 in the ER (*D*) and Golgi apparatus (*E*) after photobleaching. *F*, apoE4 has a prolonged half-maximal fluorescence recovery time in the Golgi apparatus. EGFP-apoE3, $n = 15$ experiments (98 cells) for ER; $n = 16$ experiments (102 cells) for Golgi apparatus; EGFP-apoE4, $n = 15$ experiments (97 cells) for ER; $n = 16$ experiments (110 cells) for Golgi apparatus. Values are the mean ± S.D. *, $p < 0.001$ *versus* apoE3 (two-tailed *t* test).

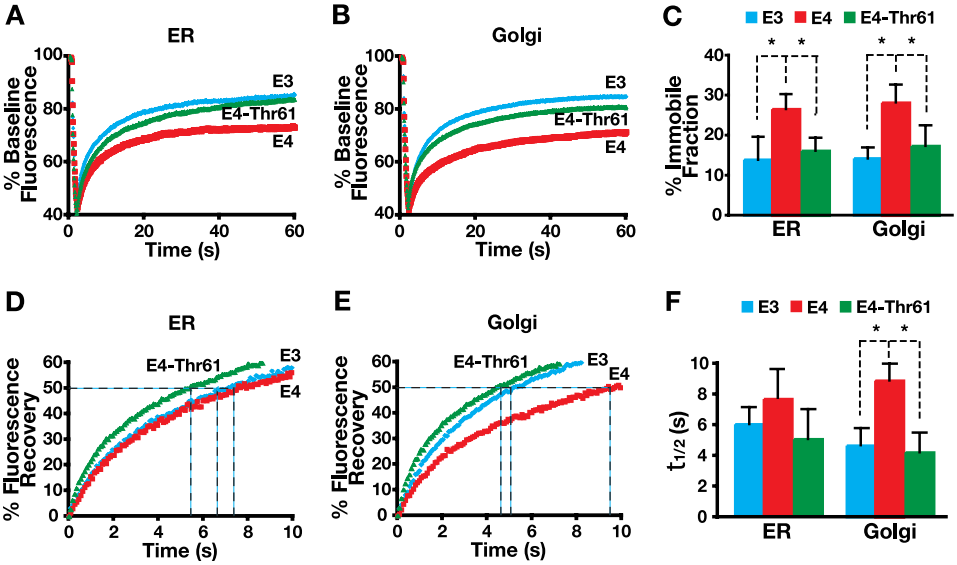

FIGURE 4. **Domain interaction is responsible for the decreased fluorescence recovery and impaired recovery kinetics of EGFP-apoE4.** *A* and *B*, disrupting domain interaction with the R61T mutation in apoE4 abolishes differences in the fluorescence recovery plateau between EGFP-apoE3 and EGFP-apoE4 in the ER (*A*) and Golgi apparatus (*B*) of Neuro-2a cells. *C*, the immobile fraction of EGFP-apoE4-R61T is similar to that of EGFP-apoE3 in the ER and Golgi apparatus. *D* and *E*, fluorescence recovery kinetics of EGFP-apoE4-R61T and EGFP-apoE3 are similar in the ER (*D*) and Golgi apparatus (*E*) of Neuro-2a cells. *F*, the recovery times of EGFP-apoE4-R61T are similar to those of EGFP-apoE3 in both the ER and Golgi apparatus. EGFP-apoE3, $n = 15$ experiments (98 cells) for ER; $n = 16$ experiments (102 cells) for Golgi apparatus; EGFP-apoE4, $n = 15$ experiments (97 cells) for ER; $n = 16$ experiments (110 cells) for Golgi apparatus. EGFP-apoE4-R61T: $n = 8$ experiments (51 cells) for ER; $n = 9$ experiments (63 cells) for Golgi apparatus. Values are the mean ± S.D. *, $p < 0.001$ (two-tailed *t* test).

ever, in the ER, half-maximal recovery times did not differ significantly between EGFP-apoE3 (6.9 ± 1.1 s) and EGFP-apoE4 (7.6 ± 2.1 s) (Fig. 3*F*). These findings suggest differences in the trafficking of apoE3 and apoE4 within the secretory pathway that specifically affect their transition through the Golgi apparatus.

Domain Interaction Impairs the Intracellular Trafficking of ApoE4 in Neuro-2a Cells—The transit time of protein cargoes through the secretory pathway is determined by several quality-control steps and is dependent on protein structure and proper folding (27–31). We hypothesized that domain interaction was responsible for the impaired intracellular trafficking of apoE4. To test this, we conducted FRAP measurements in Neuro-2a cells stably expressing EGFP-apoE4 fusion proteins carrying the R61T point mutation, which abolishes domain interaction (9, 10). The fluorescence recovery plateau of EGFP-apoE4-R61T was significantly higher than that of EGFP-apoE4 and comparable with that of EGFP-apoE3 in both the ER and Golgi apparatus (Fig. 4, *A* and *B*). EGFP-apoE4-R61T reached recovery plateau levels of 83.8 ± 3.2% in the ER and 82.5 ± 5.1% in the

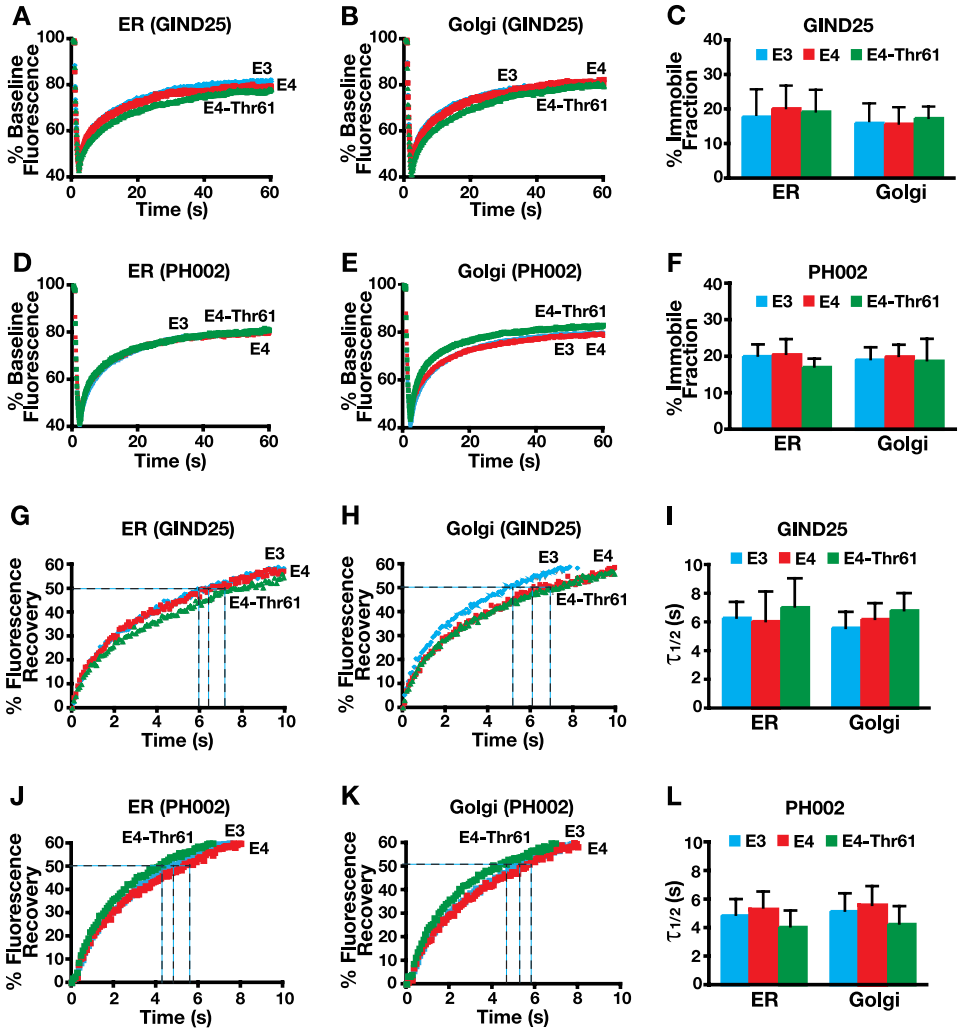

FIGURE 5. **The structure correctors GIND25 and PH002 rescue the impaired intracellular trafficking of EGFP-apoE4 in Neuro-2a cells.** *A*, *B*, *D*, and *E*, after incubation with 1 μM GIND25 or 100 nM PH002 for 72 h, the fluorescence recovery plateaus of EGFP-apoE3, EGFP-apoE4, and EGFP-apoE4-R61T are similar in the ER (*A* and *D*) and Golgi apparatus (*B* and *E*). *C* and *F*, treatment with GIND25 (1 μM) or PH002 (100 nM) abolishes differences in the immobile fractions of EGFP-apoE3, EGFP-apoE4, and EGFP-apoE4-R61T in the ER and Golgi apparatus. *G*, *H*, *J*, and *K*, after incubation with 1 μM GIND25 or 100 nM PH002 for 72 h, the recovery kinetics of EGFP-apoE4 are comparable with those of EGFP-apoE3 and EGFP-apoE4-R61T in the ER (*G* and *J*) and Golgi apparatus (*H* and *K*). *I* and *L*, GIND25 (1 μM) and PH002 (100 nM) treatment also abolish the differences in half-maximal fluorescence recovery times of EGFP-apoE3, EGFP-apoE4, and EGFP-apoE4-R61T. EGFP-apoE3: GIND25, $n = 5$ experiments (30 cells); PH002, $n = 5$ experiments (30 cells) for ER; GIND25, $n = 5$ experiments (25 cells); PH002, $n = 5$ experiments (30 cells) for Golgi apparatus; EGFP-apoE4: GIND25, $n = 5$ experiments (26 cells); PH002, $n = 5$ experiments (30 cells) for ER; GIND25, $n = 5$ experiments (25 cells); PH002, $n = 5$ experiments (30 cells) for Golgi apparatus; EGFP-apoE4-R61T: GIND25, $n = 5$ experiments (28 cells); PH002, $n = 5$ experiments (30 cells) for ER; GIND25, $n = 5$ experiments (25 cells); PH002, $n = 5$ experiments (30 cells) for Golgi apparatus. Values are the mean ± S.D.

Golgi apparatus; these values were similar to those of EGFP-apoE3 (86.1 ± 5.7 and 85.7 ± 2.8%) and differed significantly from those of EGFP-apoE4 (73.3 ± 3.7 and 71.7 ± 4.4%). Correspondingly, the immobile fraction of EGFP-apoE4-R61T in the ER (16.2 ± 3.2%) and Golgi apparatus (17.4 ± 5.1%) was about 60% that of EGFP-apoE4 (Fig. 4*C*); these values were comparable with those of EGFP-apoE3.

Consistent with the similarity of the immobile fraction, the recovery kinetics of EGFP-apoE4-R61T and EGFP-apoE3 were similar in the ER (4.9 ± 2.1 *versus* 5.9 ± 1.1 s, respectively) and Golgi apparatus (4.1 ± 1.1 *versus* 4.7 ± 1.1 s) (Fig. 4, *D–F*). Like EGFP-apoE3, EGFP-apoE4-R61T had significantly faster recovery kinetics in the Golgi apparatus than EGFP-apoE4 (4.1 ± 1.1 *versus* 8.9 ± 2 s) (Fig. 4*F*). Thus, the lower mobility of EGFP-apoE4 molecules in the Golgi apparatus appears to be dependent on domain interaction.

Abolishing Domain Interaction with Small-molecule Structure Correctors Rescues the Impaired Intracellular Trafficking of ApoE4 in Neuro-2a Cells—Next, we incubated EGFP-apoE4-expressing cells with 1 μM GIND25 (36) or 100 nM PH002, two small-molecule compounds that disrupt domain interaction, to assess their ability to rescue the impaired intracellular trafficking of EGFP-apoE4. In cells treated for 72 h with GIND25, the fluorescence recovery plateau of EGFP-apoE4 (ER: 76.7 ± 7.6%, Golgi apparatus: 81.9 ± 5.5%) was similar to that of EGFP-apoE3 (ER, 79.4 ± 8.6%; Golgi apparatus, 81.5 ± 5.9%) and EGFP-apoE4-R61T (ER, 77.8 ± 7.3%; Golgi apparatus, 79.9 ± 3.8%) (Fig. 5, *A* and *B*). Likewise, after PH002 treatment, all three forms of apoE had similar fluorescence recovery plateaus (EGFP-apoE4: ER, 79.3 ± 3.9%; Golgi apparatus, 79.9 ± 3%; EGFP-apoE3: ER, 79.8 ± 2.9%; Golgi apparatus, 80.7 ± 3.2%; EGFP-apoE4-R61T: ER, 82.8 ± 2.11%; Golgi apparatus, 81.1 ±

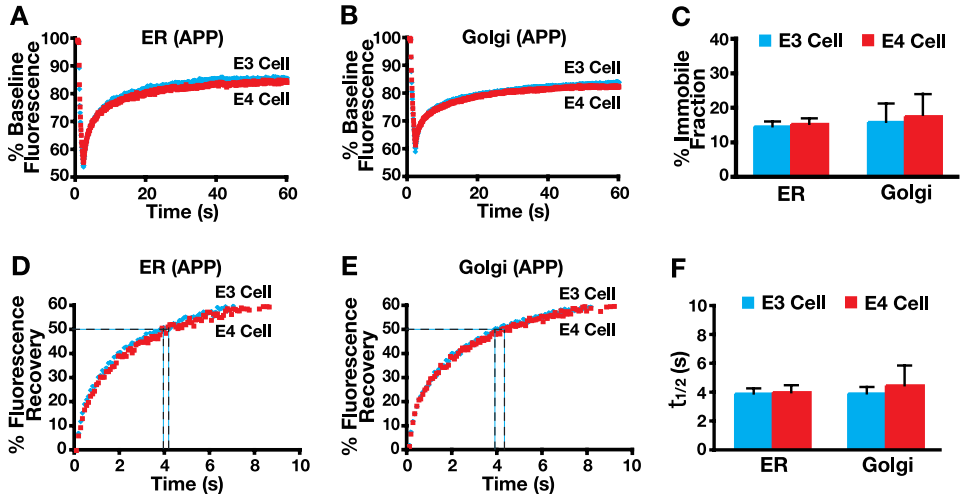

FIGURE 6. **The intracellular trafficking of APP-EGFP in Neuro-2a cells is not affected by apoE4.** *A–C*, expression of wild type apoE4 does not alter FRAP in the ER (*A*) and Golgi apparatus (*B*) and the immobile fraction (*C*) of APP-EGFP. *D–F*, expression of wild type apoE4 does not alter the recovery kinetics of APP-EGFP in the ER (*D*) and Golgi apparatus (*E*) and the half-maximal fluorescence recovery times of APP-EGFP (*F*). $n = 3$ experiments; 8–10 cells were analyzed in each experiment. Values are the mean ± S.D.

5.8%) (Fig. 5, *D* and *E*). Accordingly, the immobile fractions in the ER and Golgi apparatus of apoE-expressing Neuro-2a cells treated with the compounds were indistinguishable (Fig. 5, *C* and *F*). The fact that treatment with small molecule structure correctors did not alter the extent of fluorescence recovery in EGFP-apoE3- and EGFP-apoE4-R61T-expressing cells indicates that both GIND25 and PH002 specifically affect apoE4 structure in Neuro-2a cells, thereby rescuing the impaired intracellular trafficking of apoE4.

GIND25 (1 μM) and PH002 (100 nM) also rectified the slower fluorescence recovery kinetics of EGFP-apoE4 molecules in the Golgi apparatus (Fig. 5, *G*, *H*, *J*, and *K*), corroborating the above finding that the domain interaction is responsible for slowed apoE4 kinetics within the Golgi apparatus. In GIND25- and PH002-treated cells, half-maximal recovery times of EGFP-apoE4 were comparable with those of EGFP-apoE3 and EGFP-apoE4-R61T in the ER and Golgi apparatus (Fig. 5, *I* and *L*). Again, treatment with small-molecule structure correctors did not alter the fluorescence recovery kinetics of EGFP-apoE3 and EGFP-apoE4-R61T, indicating that these compounds rescued the intracellular trafficking impairment through specific effects on apoE4 domain interaction.

ApoE4 Does Not Affect the Intracellular Trafficking of APP-EGFP in Neuro-2a Cells—To determine whether apoE4 impairs the trafficking of other proteins, we measured the intracellular transit of APP-EGFP, another protein related to AD pathogenesis. Neuro-2a cells stably expressing untagged apoE3 or apoE4 (24) were transiently transfected with APP-EGFP. APP-EGFP reached similar fluorescence recovery plateau levels in the ER (apoE3 cells, 85.7 ± 1.9%; apoE4 cells, 84.4 ± 1.6%) and Golgi apparatus (apoE3 cells, 84.4 ± 5.3%; apoE4 cells, 82.6 ± 6.8%) (Fig. 6, *A* and *B*). Interestingly, these values were similar to those of EGFP-apoE3 (ER, 86.1%; Golgi apparatus, 85.7%) (Fig. 3) and EGFP-apoE4-R61T (ER, 83.8%; Golgi apparatus, 82.55%) (Fig. 4) but were significantly higher than that of EGFP-apoE4 (ER, 73.3%; Golgi apparatus, 71.7%) (Fig. 3). Correspondingly, the immobile fractions of APP-EGFP were comparable in the ER (apoE3 cells, 14.3 ± 1.9%; apoE4 cells, 15.6 ± 1.6%) and Golgi apparatus (apoE3 cells, 15.6 ± 5.3%; apoE4 cells, 17.4 ± 6.8%) (Fig. 6*C*). The kinetics of the fluorescence recovery of APP-EGFP were also comparable in the ER (apoE3 cells, 3.8 ± 0.3 s; apoE4 cell,: 3.9 ± 0.5 s) and Golgi apparatus (apoE3 cells, 3.8 ± 0.4 s; apoE4 cells, 4.4 ± 1.3 s) (Fig. 6, *D–F*). Thus, apoE4 does not affect the intracellular trafficking of APP-EGFP.

EGFP-apoE4 Has a Lower Diffusion Coefficient D Than EGFP-apoE3—To minimize interexperimental variations and to allow comparison of our data with other studies using different cell lines and experimental conditions, we calculated the diffusion coefficient *D* for the EGFP-apoE fusion proteins and APP-EGFP in the ER and Golgi apparatus (32). The lateral mobility of EGFP-apoE4 was 50% lower than that of EGFP-apoE3 in the Golgi apparatus (Fig. 7*A*), reflecting the slowed kinetics of its fluorescence recovery (Fig. 3). Decreased lateral mobility of EGFP-apoE4 was rectified by incubation with GIND25 and PH002 (Fig. 7, *B* and *C*). The diffusion coefficient *D* did not differ between EGFP-apoE4 and EGFP-apoE3 in the ER in the absence or presence of GIND25 or PH002 (Fig. 7, *A–C*). Furthermore, apoE4 did not affect the diffusion coefficient *D* of APP-EGFP in the ER or Golgi apparatus (Fig. 7*D*), suggesting that apoE4 does not alter general protein trafficking in neuronal cells.

We also compared the diffusion coefficient *D* of different EGFP-apoE molecules and APP-EGFP in Neuro-2a cells with the reported mobility of other GFP-tagged proteins in other cell lines (27–31). The values for EGFP-apoE and APP-EGFP were similar to those of other GFP fusion proteins in the ER and Golgi apparatus (Table 1).

Structure-dependent Impairment of ApoE4 Intracellular Trafficking Occurs in Mouse Primary Hippocampal Neurons—We then determined whether the structure-dependent impairment of apoE4 intracellular trafficking also occurs in mouse primary hippocampal neurons. Primary neurons were transduced with Sindbis virus expressing EGFP-apoE3, EGFP-apoE4, or EGFP-apoE4-R61T (Fig. 8, *A–C*). Because of the difficulty of identifying the Golgi apparatus in primary neurons, we measured general apoE trafficking in the soma. The immo-

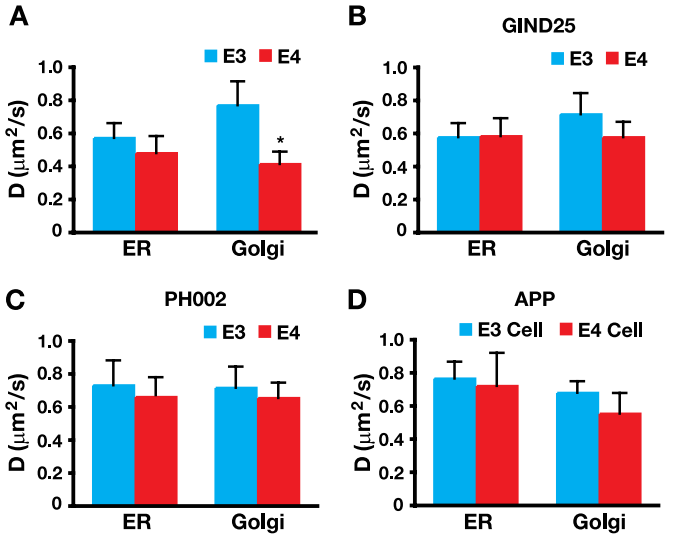

FIGURE 7. **EGFP-apoE4 has a lower diffusion coefficient *D* than EGFP-apoE3, and treatment with GIND25 and PH002 (structure correctors) abolishes the difference.** *A*, the diffusion coefficient *D* of EGFP-apoE4 is ~50% lower than that of EGFP-apoE3 in the Golgi apparatus of Neuro-2a cells. EGFP-apoE3: $n = 15$ experiments (98 cells) for ER; $n = 16$ experiments (102 cells) for Golgi apparatus. EGFP-apoE4: $n = 15$ experiments (97 cells) for ER; $n = 16$ experiments (110 cells) for Golgi apparatus. Values are the mean ± S.D. *, $p < 0.001$ *versus* apoE3 (two-tailed *t* test). *B* and *C*, treatment with GIND25 (1 μM) and PH002 (100 nM) for 72 h increased the diffusion coefficient *D* of EGFP-apoE4 to levels similar to that of EGFP-apoE3 in the Golgi apparatus and did not affect the diffusion factor in the ER. EGFP-apoE3: GIND25, $n = 5$ experiments (30 cells); PH002, $n = 5$ experiments (30 cells) for ER; GIND25, $n = 5$ experiments (25 cells); PH002, $n = 5$ experiments (30 cells) for Golgi apparatus. EGFP-apoE4: GIND25, $n = 5$ experiments (26 cells) for ER; PH002, $n = 5$ experiments (30 cells); GIND25, $n = 5$ experiments (25 cells); Ph002, $n = 5$ experiments (30 cells) for Golgi apparatus. Values are the mean ± S.D. *D*, the diffusion coefficient *D* of APP-EGFP was similar in the presence of apoE3 or apoE4. $n = 3$ experiments each in apoE3 and apoE4 cells (8–10 cells per experiment). Values are the mean ± S.D.

TABLE 1

Lateral velocities of EGFP chimeras in different cells at 37 °C as determined by FRAP

VSVG, vesicular stomatitis virus glycoprotein.

Molecule	*D*
	$\mu m^2 s^{-1}$
GFP in cytoplasm	25[a]
GFP in ER lumen	5–10[b]
ER	
VSVG tsO45-GFP	0.49[c]
Signal recognition particle β-subunit-GFP	0.26[c]
EGFP-apoE3	0.56
EGFP-apoE4	0.47
APP-EGFP (in the presence of apoE3)	0.75
APP-EGFP (in the presence of apoE4)	0.71
Golgi apparatus	
KDELR-GFP	0.46[d]
Manosidase II-GFP	0.32[d]
Galactosyltransferase-GFP	0.54[d]
EGFP-apoE3	0.76
EGFP-apoE4	0.41
APP-EGFP (in the presence of apoE3)	0.67
APP-EGFP (in the presence of apoE4)	0.55
Plasma membrane	
E-cadherin-GFP	0.03–0.04[e]

[a] From Ref. 51.
[b] From Ref. 52.
[c] From Ref. 53.
[d] From Ref. 54.
[e] From Ref. 55.

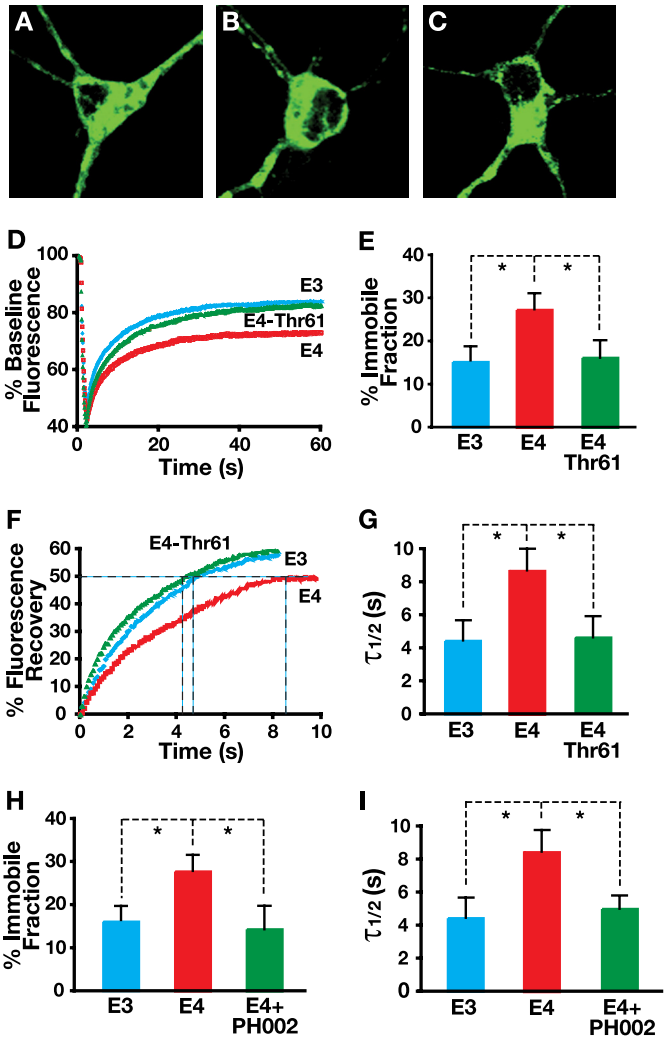

FIGURE 8. **Structure-dependent impairment of the intracellular trafficking of apoE4 in mouse primary hippocampal neurons.** *A–C*, representative confocal images of apoE knock-out mouse primary hippocampal neurons expressing EGFP-apoE3 (*A*), EGFP-apoE4 (*B*), or EGFP-apoE4-R61T (*C*) are shown. *D*, FRAP measurements of EGFP-apoE3, EGFP-apoE4, and EGFP-apoE4-R61T in primary neurons are shown. *E*, the immobile fraction of EGFP-apoE4 is ~100% higher than that of EGFP-apoE3 and EGFP-apoE4-R61T. *F*, fluorescence recovery kinetics of EGFP-apoE3, EGFP-apoE4, and EGFP-apoE4-R61T in primary neurons after photobleaching are shown. *G*, apoE4 is associated with a longer half-maximal fluorescence recovery time than EGFP-apoE3 and EGFP-apoE4-R61T. *H* and *I*, the structure corrector PH002 (100 nM for 2 days) rescues the impaired intracellular trafficking of EGFP-apoE4 in primary neurons. EGFP-apoE3: $n = 4$ experiments (28 cells); EGFP-apoE4: $n = 4$ experiments (26 cells); EGFP-apoE4-R61T: $n = 3$ experiments (23 cells); EGFP-apoE4 + PH002: $n = 3$ experiments (21 cells). Values are the mean ± S.D. *, $p < 0.001$ (two-tailed *t* test).

bile fraction was about 100% higher in primary neurons expressing EGFP-apoE4 than in those expressing EGFP-apoE3 (27.5 ± 4.8% *versus* 14.6 ± 4.1%) (Fig. 8, *D* and *E*). Likewise, the half-maximal recovery time of EGFP-apoE4 was significantly slower in primary neurons expressing EGFP-apoE4 than in those expressing EGFP-apoE3 (8.6 ± 1.7 *versus* 4.2 ± 1.3 s) (Fig. 8, *F* and *G*). Importantly, the immobile fraction (15.5 ± 4.5%) and the half-maximal recovery time (4.6 ± 1.4 s) of EGFP-apoE4-R61T were comparable with those of EGFP-apoE3 in primary neurons (Fig. 8, *D–G*). Furthermore, treatment of primary neurons with PH002 (100 nM) rescued the impairment of intraneuronal trafficking of EGFP-apoE4 (Fig. 8, *H* and *I*).

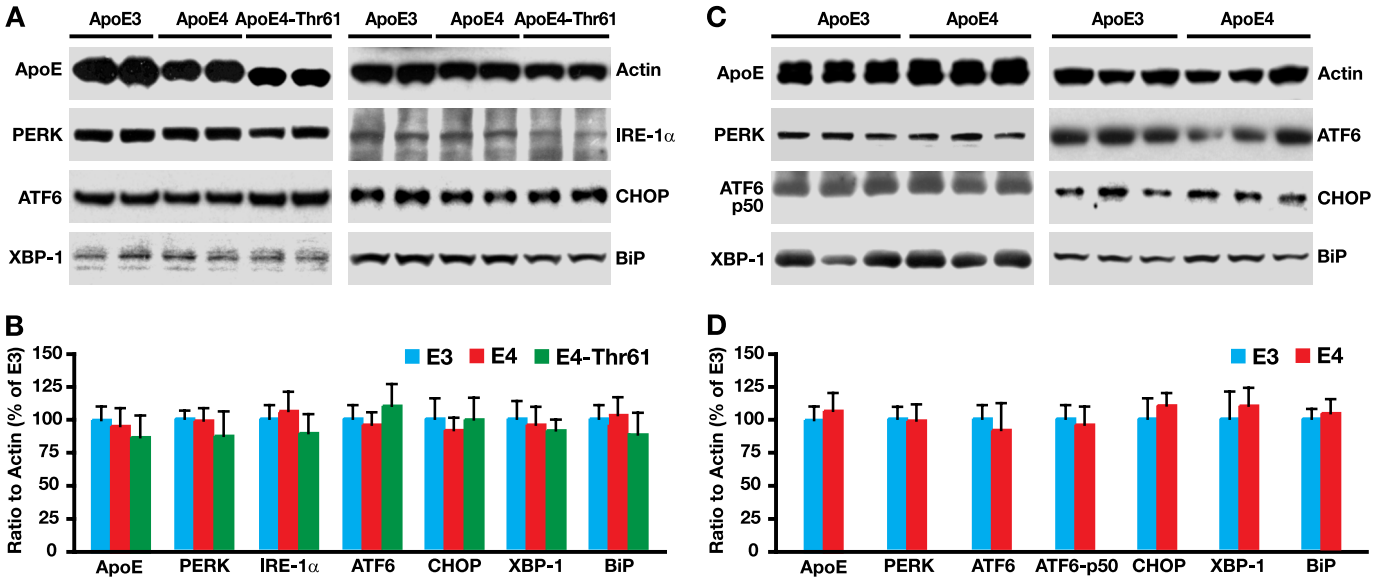

FIGURE 9. **ApoE4 does not cause ER stress in neuronal cells.** *A*, different ER stress sensors and mediators were analyzed by Western blot in Neuro-2a cell lysates. *B*, the levels of ER stress sensors and mediators in different Neuro-2a cell lysates were normalized to actin and are presented as the percentage of cells expressing apoE3. *C*, ER stress sensors and mediators were analyzed by Western blot in brain lysates of female NSE-apoE3 and NSE-apoE4 mice at 6 months of age. *D*, the levels of ER stress sensors and mediators in different mouse brain lysates were normalized to actin and presented as the percentage of mice expressing apoE3. $n = 3–5$ for each protein and genotype. Values are the mean ± S.D. *PERK*, double stranded RNA activated protein kinase-like ER kinase; *XBP-1*, X-box-binding protein 1; *ATF6*, activating transcription factor 6; *IRE-1α*, inositol-requiring enzyme 1α; *CHOP*, C/EBP homologous protein; BiP, immunoglobulin heavy chain binding protein.

ApoE4 Does Not Cause ER Stress in Neuronal Cells—We reported that apoE4 causes ER stress in astrocytes (37). We then determined whether apoE4 intracellular trafficking impairment leads to ER stress in neuronal cells by measuring the protein levels of ER stress sensors and mediators (37), including double stranded RNA activated protein kinase-like ER kinase (*PERK*), inositol-requiring enzyme 1α (*IRE-1α*), activating transcription factor 6 (*ATF6*), C/EBP homologous protein (*CHOP*), X-box-binding protein 1 (*XBP-1*), and immunoglobulin heavy chain binding protein (*BiP*). There were no significant differences in protein levels of any of these ER stress sensors or mediators, as determined by Western blot, in Neuro-2a cells expressing apoE3 or apoE4 (Fig. 9, *A* and *B*) and in brains of transgenic mice specifically expressing apoE3 or apoE4 in neurons (Fig. 9, *C* and *D*).

Rescuing the Impaired Intracellular Trafficking of ApoE4 by a Structure Corrector Abolishes Its Detrimental Effect on Neurite Outgrowth—Time-lapse imaging of live Neuro-2a cells revealed that EGFP-apoE was constantly moving from the soma to neurites, with some apoE4 molecules being immobile (supplemental movie). Because neuronal apoE4 inhibits neurite outgrowth compared with apoE3 (38), we tested whether rescuing the impaired intracellular trafficking of apoE4 prevents neuronal cells from apoE4 detrimental effect on neurite outgrowth. Indeed, Neuro-2a cells expressing apoE4 had shorter neurites than those expressing apoE3 (Fig. 10, *A*, *B*, and *D*). Treatment with PH002, which rescued intracellular trafficking of apoE4 (Figs. 5 and 8), stimulated neurite outgrowth in apoE4-expressing cells to a level similar to that in cells expressing apoE3 (Fig. 10, *A*, *C*, and *D*). PH002 did not affect neurite outgrowth of cells expressing apoE3 (Fig. 10*D*), suggesting a specific effect on apoE4.

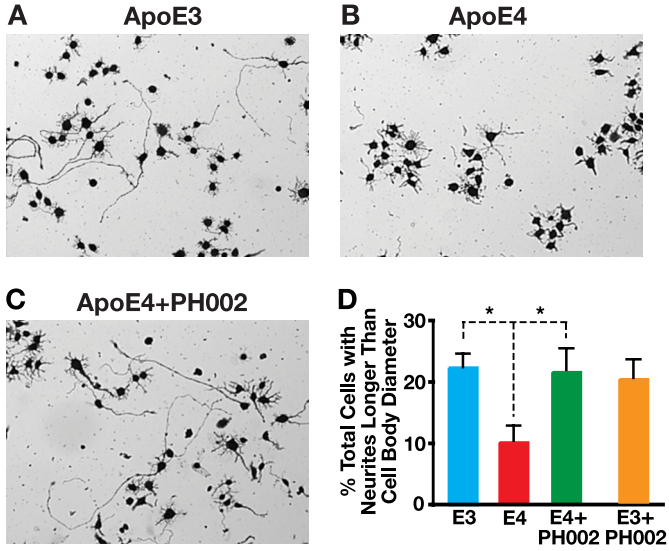

FIGURE 10. **Rescuing the impaired intracellular trafficking of apoE4 with a structure corrector abolishes the apoE4 detrimental effect on neurite outgrowth.** *A–C*, representative images of Neuro-2a cells expressing apoE3 (*A*), apoE4 (*B*), or apoE4 treated with PH002 (100 nM for 3 days) (*C*) in differentiation medium for 3 days are shown. *D*, quantification of neurite outgrowth in different Neuro-2a cells is shown. $n = 4–6$ per genotype and treatment. Values are the mean ± S.D. *, $p < 0.01$ (two-tailed *t* test).

Rescuing the Impaired Intracellular Trafficking of ApoE4 by a Structure Corrector Abolishes Its Detrimental Effect on Dendritic Spine Development—ApoE4 decreases the numbers of dendritic spines and synapses in primary neuronal cultures and in the brains of transgenic or gene-targeted mice (34, 39, 40). We determined whether rescuing the impaired intracellular trafficking of apoE4 protects neurons from this detrimental effect. Dendritic spine density was significantly lower in hippocampal neurons cultured from neuron-specific NSE-apoE4 transgenic mice than in those cultured from NSE-apoE3 mice

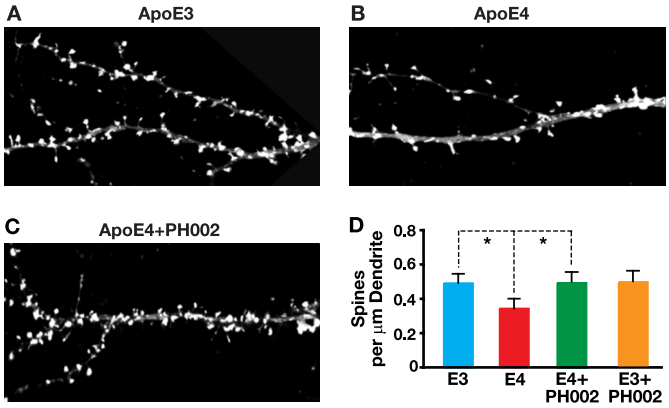

FIGURE 11. **Rescuing the impaired intracellular trafficking of apoE4 with a structure corrector abolishes the apoE4 detrimental effect on dendritic spine development.** *A–C*, shown are representative confocal images of mouse hippocampal neurons expressing apoE3 (*A*), apoE4 (*B*), or apoE4 treated with PH002 (*C*). Primary neurons were transiently transfected with EGFP-β-actin at 5 DIV to highlight the dendritic spines. At 11 DIV, some neurons were treated with PH002 (100 nM) for 3 days). At 14 DIV, all primary neurons were fixed, and confocal images were obtained with a 60× oil objective lens were collected. *D*, quantification of dendritic spine densities in different primary neurons is shown. ApoE3: $n = 28$ dendrites from 14 neurons; apoE4: $n = 26$ dendrites from 12 neurons; apoE4 + PH002: $n = 23$ dendrites from 11 neurons; apoE3 + PH002: $n = 27$ dendrites from 15 neurons. Values are the mean ± S.D. *, $p < 0.01$ (two-tailed *t* test).

(Fig. 11, *A*, *B*, and *D*). Treatment of primary neurons expressing apoE4 with PH002, which rescued intracellular trafficking of apoE4 (Figs. 5 and 8), increased the dendritic spine density to a level similar to that of neurons expressing apoE3 (Fig. 11, *A*, *C*, and *D*). PH002 did not affect dendritic spine density of apoE3-expressing neurons (Fig. 11*D*), again suggesting a specific effect on apoE4.

DISCUSSION

This study shows that a structural feature of apoE4 characterized by domain interaction impairs the trafficking of apoE4 in the ER and Golgi apparatus, the two major processing and quality-control compartments of newly synthesized proteins in the secretory pathway. Preventing apoE4 domain interaction, either genetically or pharmacologically, abolished the impairment. Thus, correcting the pathological structure of apoE4 by disrupting domain interaction is a potentially promising strategy for treating or preventing AD related to apoE4 (14–16).

Our findings have implications for understanding how apoE4 contributes to AD pathogenesis. First, the biological difference between apoE4 and apoE3 emerged early during their synthesis in the ER and resulted from apoE4 domain interaction. Given the importance of apoE in synaptogenesis and in neuronal plasticity, repair, and remodeling, the impairment of intracellular trafficking and the retention of apoE4 molecules could have dire consequences over time, especially on neurons with long axonal projections and high plasticity, and could contribute to AD pathogenesis. For example, the impaired trafficking of apoE4 in neuronal cells could contribute to apoE4-induced inhibition of neurite outgrowth and impairment of synaptogenesis (34, 38–43). In fact, rescuing the impaired intracellular trafficking of apoE4 with a small-molecule structure corrector abolished its detrimental effects on neurite outgrowth and dendritic spine development.

Second, in previous studies we showed that neuronal apoE4 is more susceptible than neuronal apoE3 to proteolysis, resulting in a greater abundance of neurotoxic apoE4 fragments (44–46). The immobile apoE4 molecules retained in the ER and Golgi apparatus could be targeted by the apoE-cleaving enzyme to generate neurotoxic apoE fragments. In support of this possibility, the retention of immobile apoE4 molecules reported here and proteolysis of apoE4 in neuronal cells (14–16) are both dependent on domain interaction.

We previously reported that apoE4 causes ER stress in astrocytes (37). However, the impairment of apoE4 trafficking did not lead to ER stress in neuronal cells in the current study. These findings suggest that neurons and astrocytes respond differently to apoE4. Alternatively, neuronal apoE4 and astrocytic apoE4 act differently in their pathogenic roles, as suggested recently (16, 47). For example, neuronal apoE4 is less lipidated than neuronal apoE3 (13), whereas astrocytic apoE4 and apoE3 have no difference in lipidation (48). On the other hand, astrocytic apoE4 causes ER stress (37), whereas neuronal apoE4 does not. Unraveling the mechanisms for these differences should shed light on cell type-specific responses to apoE4 and its role in AD pathogenesis.

How could domain interaction impair the intracellular trafficking of apoE4? At least two possibilities must be considered. First, domain interaction might cause apoE4 to be recognized as a misfolded protein by the protein quality-control machinery in the ER and Golgi apparatus and retained for chaperone-assisted refolding and, if not successful, eventually for degradation. Second, domain interaction decreases lipid binding of apoE4 in neuronal cells (13, 37). "Poorly lipidated" apoE4 might be recognized by the cellular lipoprotein assembly machinery as an immature product and retained for further lipidation and potentially also for degradation. Importantly, apoE4 did not impair the mobility of the secretory protein APP. Thus, the impaired trafficking of apoE4 more likely reflects retention and slowed transit of apoE4 itself rather than a general effect on the transit of protein cargoes through the secretory pathway.

Our findings also suggest a new strategy for developing anti-AD therapeutics targeting apoE4. Domain interaction is a major biophysical property of apoE4. It occurs to a significantly lesser extent in apoE2 and apoE3 (9–11) and is responsible for several detrimental neuropathological effects of apoE4 (11, 14–16). The R61T mutation in apoE4, which eliminates domain interaction, abolished the impairment of intracellular trafficking. Consistent with this finding, GIND25 and PH002 rescued the impairment of apoE4 trafficking in neuronal cells and abolished apoE4 detrimental effects on neurite outgrowth and dendritic spine development. GIND25 and PH002 block apoE4 domain interaction and convert apoE4 to a molecule that resembles apoE3 both structurally and functionally (36). Thus, small-molecule structure correctors of apoE4 might help prevent or treat AD in apoE4 carriers. Currently, the structure corrector concept in drug development, targeting mutant cystic fibrosis transmembrane conductance regulator and p53, is being tested in clinical trials (49, 50).

Acknowledgments—We thank Linda Turney for manuscript preparation, John Carroll and Chris Goodfellow for graphics, and Stephen Ordway and Gary Howard for editorial assistance.

REFERENCES

1. Mahley, R. W. (1988) *Science* **240,** 622–630
2. Weisgraber, K. H. (1994) *Adv. Protein Chem.* **45,** 249–302
3. Corder, E. H., Saunders, A. M., Strittmatter, W. J., Schmechel, D. E., Gaskell, P. C., Small, G. W., Roses, A. D., Haines, J. L., and Pericak-Vance, M. A. (1993) *Science* **261,** 921–923
4. Saunders, A. M., Strittmatter, W. J., Schmechel, D., George-Hyslop, P. H., Pericak-Vance, M. A., Joo, S. H., Rosi, B. L., Gusella, J. F., Crapper-MacLachlan, D. R., Alberts, M. J., Hulette, C., Crain, B., Goldgaber, D., and Roses, A. D. (1993) *Neurology* **43,** 1467–1472
5. Strittmatter, W. J., Saunders, A. M., Schmechel, D., Pericak-Vance, M., Enghild, J., Salvesen, G. S., and Roses, A. D. (1993) *Proc. Natl. Acad. Sci. U.S.A.* **90,** 1977–1981
6. Farrer, L. A., Cupples, L. A., Haines, J. L., Hyman, B., Kukull, W. A., Mayeux, R., Myers, R. H., Pericak-Vance, M. A., Risch, N., and Van Duijn, C. M. (1997) *J. Am. Med. Assoc.* **278,** 1349–1356
7. Morrow, J. A., Hatters, D. M., Lu, B., Hochtl, P., Oberg, K. A., Rupp, B., and Weisgraber, K. H. (2002) *J. Biol. Chem.* **277,** 50380–50385
8. Hatters, D. M., Peters-Libeu, C. A., and Weisgraber, K. H. (2005) *J. Biol. Chem.* **280,** 26477–26482
9. Dong, L. M., Wilson, C., Wardell, M. R., Simmons, T., Mahley, R. W., Weisgraber, K. H., and Agard, D. A. (1994) *J. Biol. Chem.* **269,** 22358–22365
10. Dong, L. M., and Weisgraber, K. H. (1996) *J. Biol. Chem.* **271,** 19053–19057
11. Zhong, N., and Weisgraber, K. H. (2009) *J. Biol. Chem.* **284,** 6027–6031
12. Raffai, R. L., Dong, L. M., Farese, R. V., Jr., and Weisgraber, K. H. (2001) *Proc. Natl. Acad. Sci. U.S.A.* **98,** 11587–11591
13. Xu, Q., Brecht, W. J., Weisgraber, K. H., Mahley, R. W., and Huang, Y. (2004) *J. Biol. Chem.* **279,** 25511–25516
14. Mahley, R. W., Weisgraber, K. H., and Huang, Y. (2006) *Proc. Natl. Acad. Sci. U.S.A.* **103,** 5644–5651
15. Huang, Y. (2006) *Curr. Opin. Drug Discov. Devel.* **9,** 627–641
16. Huang, Y. (2010) *Trends Mol. Med.* **16,** 287–294
17. Elshourbagy, N. A., Liao, W. S., Mahley, R. W., and Taylor, J. M. (1985) *Proc. Natl. Acad. Sci. U.S.A.* **82,** 203–207
18. Linton, M. F., Gish, R., Hubl, S. T., Bütler, E., Esquivel, C., Bry, W. I., Boyles, J. K., Wardell, M. R., and Young, S. G. (1991) *J. Clin. Invest.* **88,** 270–281
19. Boyles, J. K., Pitas, R. E., Wilson, E., Mahley, R. W., and Taylor, J. M. (1985) *J. Clin. Invest.* **76,** 1501–1513
20. Pitas, R. E., Boyles, J. K., Lee, S. H., Foss, D., and Mahley, R. W. (1987) *Biochim. Biophys. Acta* **917,** 148–161
21. Xu, P. T., Gilbert, J. R., Qiu, H. L., Ervin, J., Rothrock-Christian, T. R., Hulette, C., and Schmechel, D. E. (1999) *Am. J. Pathol.* **154,** 601–611
22. Messmer-Joudrier, S., Sagot, Y., Mattenberger, L., James, R. W., and Kato, A. C. (1996) *Eur. J. Neurosci.* **8,** 2652–2661
23. Boschert, U., Merlo-Pich, E., Higgins, G., Roses, A. D., and Catsicas, S. (1999) *Neurobiol. Dis.* **6,** 508–514
24. Harris, F. M., Tesseur, I., Brecht, W. J., Xu, Q., Mullendorff, K., Chang, S., Wyss-Coray, T., Mahley, R. W., and Huang, Y. (2004) *J. Biol. Chem.* **279,** 3862–3868
25. Xu, Q., Bernardo, A., Walker, D., Kanegawa, T., Mahley, R. W., and Huang, Y. (2006) *J. Neurosci.* **26,** 4985–4994
26. Xu, Q., Walker, D., Bernardo, A., Brodbeck, J., Balestra, M. E., and Huang, Y. (2008) *J. Neurosci.* **28,** 1452–1459
27. Sitia, R., and Braakman, I. (2003) *Nature* **426,** 891–894
28. Römisch, K. (2004) *Traffic* **5,** 815–820
29. Anelli, T., and Sitia, R. (2008) *EMBO J.* **27,** 315–327
30. Ellgaard, L., and Helenius, A. (2003) *Nat. Rev. Mol. Cell Biol.* **4,** 181–191
31. Trombetta, E. S., and Parodi, A. J. (2003) *Annu. Rev. Cell Dev. Biol.* **19,** 649–676
32. Diliberto, E. J., Jr., and Axelrod, J. (1976) *J. Neurochem.* **26,** 1159–1165
33. Li, G., Bien-Ly, N., Andrews-Zwilling, Y., Xu, Q., Bernardo, A., Ring, K., Halabisky, B., Deng, C., Mahley, R. W., and Huang, Y. (2009) *Cell Stem Cell* **5,** 634–645
34. Brodbeck, J., Balestra, M. E., Saunders, A. M., Roses, A. D., Mahley, R. W., and Huang, Y. (2008) *Proc. Natl. Acad. Sci. U.S.A.* **105,** 1343–1346
35. Chang, S., ran Ma, T., Miranda, R. D., Balestra, M. E., Mahley, R. W., and Huang, Y. (2005) *Proc. Natl. Acad. Sci. U.S.A.* **102,** 18694–18699
36. Ye, S., Huang, Y., Müllendorff, K., Dong, L., Giedt, G., Meng, E. C., Cohen, F. E., Kuntz, I. D., Weisgraber, K. H., and Mahley, R. W. (2005) *Proc. Natl. Acad. Sci. U.S.A.* **102,** 18700–18705
37. Zhong, N., Ramaswamy, G., and Weisgraber, K. H. (2009) *J. Biol. Chem.* **284,** 27273–27280
38. Bellosta, S., Nathan, B. P., Orth, M., Dong, L. M., Mahley, R. W., and Pitas, R. E. (1995) *J. Biol. Chem.* **270,** 27063–27071
39. Ji, Y., Gong, Y., Gan, W., Beach, T., Holtzman, D. M., and Wisniewski, T. (2003) *Neuroscience* **122,** 305–315
40. Dumanis, S. B., Tesoriero, J. A., Babus, L. W., Nguyen, M. T., Trotter, J. H., Ladu, M. J., Weeber, E. J., Turner, R. S., Xu, B., Rebeck, G. W., and Hoe, H. S. (2009) *J. Neurosci.* **29,** 15317–15322
41. Nathan, B. P., Bellosta, S., Sanan, D. A., Weisgraber, K. H., Mahley, R. W., and Pitas, R. E. (1994) *Science* **264,** 850–852
42. Nathan, B. P., Chang, K. C., Bellosta, S., Brisch, E., Ge, N., Mahley, R. W., and Pitas, R. E. (1995) *J. Biol. Chem.* **270,** 19791–19799
43. Holtzman, D. M., Pitas, R. E., Kilbridge, J., Nathan, B., Mahley, R. W., Bu, G., and Schwartz, A. L. (1995) *Proc. Natl. Acad. Sci. U.S.A.* **92,** 9480–9484
44. Huang, Y., Liu, X. Q., Wyss-Coray, T., Brecht, W. J., Sanan, D. A., and Mahley, R. W. (2001) *Proc. Natl. Acad. Sci. U.S.A.* **98,** 8838–8843
45. Harris, F. M., Brecht, W. J., Xu, Q., Tesseur, I., Kekonius, L., Wyss-Coray, T., Fish, J. D., Masliah, E., Hopkins, P. C., Scearce-Levie, K., Weisgraber, K. H., Mucke, L., Mahley, R. W., and Huang, Y. (2003) *Proc. Natl. Acad. Sci. U.S.A.* **100,** 10966–10971
46. Brecht, W. J., Harris, F. M., Chang, S., Tesseur, I., Yu, G. Q., Xu, Q., Dee, Fish, J., Wyss-Coray, T., Buttini, M., Mucke, L., Mahley, R. W., and Huang, Y. (2004) *J. Neurosci.* **24,** 2527–2534
47. Buttini, M., Masliah, E., Yu, G. Q., Palop, J. J., Chang, S., Bernardo, A., Lin, C., Wyss-Coray, T., Huang, Y., and Mucke, L. (2010) *Am. J. Pathol.* **177,** 563–569
48. DeMattos, R. B., Brendza, R. P., Heuser, J. E., Kierson, M., Cirrito, J. R., Fryer, J., Sullivan, P. M., Fagan, A. M., Han, X., and Holtzman, D. M. (2001) *Neurochem. Int.* **39,** 415–425
49. Kalid, O., Mense, M., Fischman, S., Shitrit, A., Bihler, H., Ben-Zeev, E., Schutz, N., Pedemonte, N., Thomas, P. J., Bridges, R. J., Wetmore, D. R., Marantz, Y., and Senderowitz, H. (2010) *J. Comput. Aided Mol. Des.* **24,** 971–991
50. Wang, W., and El-Deiry, W. S. (2008) *Curr. Opin. Oncol.* **20,** 90–96
51. Swaminathan, R., Hoang, C. P., and Verkman, A. S. (1997) *Biophys. J.* **72,** 1900–1907
52. Dayel, M. J., Hom, E. F., and Verkman, A. S. (1999) *Biophys. J.* **76,** 2843–2851
53. Nehls, S., Snapp, E. L., Cole, N. B., Zaal, K. J., Kenworthy, A. K., Roberts, T. H., Ellenberg, J., Presley, J. F., Siggia, E., and Lippincott-Schwartz, J. (2000) *Nat. Cell Biol.* **2,** 288–295
54. Cole, N. B., Smith, C. L., Sciaky, N., Terasaki, M., Edidin, M., and Lippincott-Schwartz, J. (1996) *Science* **273,** 797–801
55. Adams, C. L., Chen, Y. T., Smith, S. J., and Nelson, W. J. (1998) *J. Cell. Biol.* **142,** 1105–1119